EXTRACTING OLIVINE (FO-FA) COMPOSITIONS FROM RAMAN SPECTRAL PEAK POSITIONS. K. Kuebler, B. L. Jolliff; Alian Wang, and L. A. Haskin Dept. of Earth & Planetary Sciences & the McDonnell Center for Space Sciences, Washington University, One Brookings Drive, St. Louis, MO 63130. (kuebler@levee.wustl.edu)

Introduction. Olivine and pyroxene are two major basaltic minerals that have been identified at Gusev Crater and Meridiani Planum by the Mars Exploration Rovers [1-3]. Full petrologic characterization of a sample (rock or soil), however, requires determining the range of mineral compositions, extent of zoning, range of grain sizes, mineral associations, presence of xenocrysts, etc. Information of this sort will aid the interpretation of sample crystallization and differentiation histories and help discriminate between lithologies.

In Raman spectroscopic experiments, minerals are identified by their spectral patterns and mineral compositions can be inferred from the peak positions. Instruments currently in use or slated for impending surface exploration missions provide only average elemental compositions for relatively large rock or soil targets or bulk mineral analysis. No techniques currently in use or scheduled for flight can characterize both structure and composition of individual mineral grains, in-situ, like the Mars Microbeam Raman Spectrometer (MMRS). The MMRS is designed to take 100 spectra along a 1 cm linear traverse on the surface of a sample, with contributions from one or a few mineral phases per spectrum. We presented a method to extract structural and compositional information from the Raman spectra of quadrilateral pyroxenes in [4]. The pyroxene calibration was applied to a Raman spectroscopic study of Martian meteorite EETA79001 along with a preliminary olivine calibration, where we demonstrated the capability to discriminate related lithologies using Raman point counts [5]. This abstract presents an improved olivine calibration that will further aid sample characterization and the study of alteration processes [6, 7].

Samples. We use a combination of terrestrial, meteoritic and synthetic samples of the end-members to cover the entire range of olivine compositions (Table 1). Raman and electron microprobe (EMP) analyses were made at the same locations. We used mostly coarse-grained and unzoned samples to limit disparities that arise from the different sampling volumes of the Raman laser and EMP electron beam. Only data with good EMP totals, stoichiometry and good resolution of both the ~820 and ~850 cm^{-1} peaks (Figure 1) were used in the calibration. Olivine in lunar meteorite LAP02224,24 are smaller and unequilibrated but were chosen because they span a range of uncommon compositions Fo_{20-40}. Data from LAP were not used in the data set to derive the calibration because the Fo_{20-40} grains are too strongly zoned but are included with the data used to test the calibration.

Methods. All Raman spectra were collected on a HoloLab 5000 (Kaiser Optical Systems, Inc.) spectrometer with the 532 nm line of a frequency-doubled Nd:YAG laser, unpolarized at the sample. This spectrometer has a spectral resolution of 4-5 cm^{-1}. The wavenumber accuracy is <0.003 nm in the region of interest and is monitored for reproducibility using the 520.5 cm^{-1} Raman shift of a Si wafer. All spectra were acquired using a 20x long-working distance objective (0.4 NA), ~15 mW laser power, ~6µm beam diameter, and spectrum accumulation time of 30 seconds. All peak positions were obtained using a least squares curve-fitting subroutine with a mixed Gaussian-Lorentzian peak shape and linear baseline. We use the constraint-free iteration option in the subroutine for adjusting all parameters until convergence is attained.

The electron microprobe (EMP) data were collected with a beam current of ~30 nA, accelerating voltage of 15 kV and a defocused beam (10 µm) to better approximate the area analyzed by the Raman laser. We used the accepted chemical compositions of the synthetic end-members (microprobe standards) given in [8, 9]. The average Fo content of each sample is given in Table 1.

Raman spectrum of olivine. Detailed Raman peak assignments for forsterite can be found in [10, 11] and of olivines in general in [12]. Olivine has 81 optic modes, 36 of which are Raman-active [12, 13]. Olivine spectra (Figure 1) can be divided into 3 regions: <400 cm^{-1}, 400–800 cm^{-1}, and 800–1100 cm^{-1}. Peaks between 800 and 1100 cm^{-1} are attributed to SiO_4 internal stretching vibrational modes; the dominant feature in this region is a doublet with peaks near 820 and 850 cm^{-1} whose relative heights are a function of crystal orientation [10]. These peaks result from coupled symmetric (ν_1) and asymmetric (ν_3) vibrations of SiO_4 tetrahedra [10-16] and are readily recognized in multi-phase spectra [5, 17]. Peaks in the 400–800 cm^{-1} region are mainly from SiO_4 internal bending vibrational modes. Peaks below 400 cm^{-1} are mostly contributed by lattice modes: rotations and translations of SiO_4 units and translations of octahedral cations in the crystal lattice [12]. These are weaker peaks, not often resolved in multi-phase spectra so only the doublet in the 800 –1100 cm^{-1} region is used in the calibration. Peak positions of the doublet are observed to vary with composition despite contributions from multiple vibrational modes [11, 12, 15]. The observed range for the ~820 cm^{-1} peak position is about 10 wavenumbers: from 815.0 cm^{-1} in fayalite to 824.8 cm^{-1} in forsterite. The observed range for the ~850 cm^{-1} peak is wider: from 838.1 cm^{-1} to 856.7 cm^{-1}.

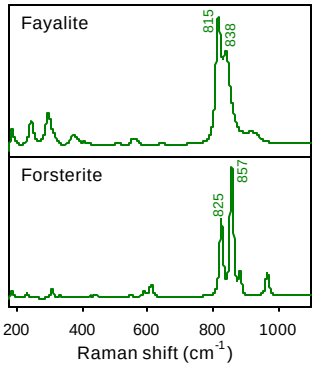

Figure 1. Raman spectra of the olivine end members fayalite and forsterite.

Both peaks are broader and thus less resolved in fayalite, presumably due to greater anharmonicity in the Si–O vibrations [18]. The positions of both of these peaks are used in what we refer to here as the 3-D calibration.

Calibration. The 3-D calibration derives from a best-fit parabola to 3 experimental parameters: the ~820 and ~850 cm^{-1} peak positions and Fo values (Fo = Mg/(Mg+Fe) in a mole; $Fo_{0.00\text{-}1.00}$) calculated from the corresponding EMP data. The parabola has the form: (1) Fo= $y_0 + a_1x + b_1y + a_2x^2 + b_2y^2$, where x is the ~850 cm^{-1} peak position and y the ~820 cm^{-1} peak position. Figure 2a shows a projection of the calibration data set onto the plane of the ~820 cm^{-1} and ~850 cm^{-1} peak positions. The central dashed line in Figure 2a is the best-fit curve to spectral peaks from the same samples. The data are constrained by a correlation between the two peaks, an equation with the form: (2) ~820 cm^{-1} peak = $y_0 + cx + dx^2$, where x is the ~850 cm^{-1} peak position. Below $Fo_{0.3}$ scattering is observed in the ~850 cm^{-1} peak positions owing to peak broadening and variations in the vibrational mixing of modes. Peaks from olivine of these compositions overlap and cannot be adequately distinguished, so they are grouped together in Figure 2a.

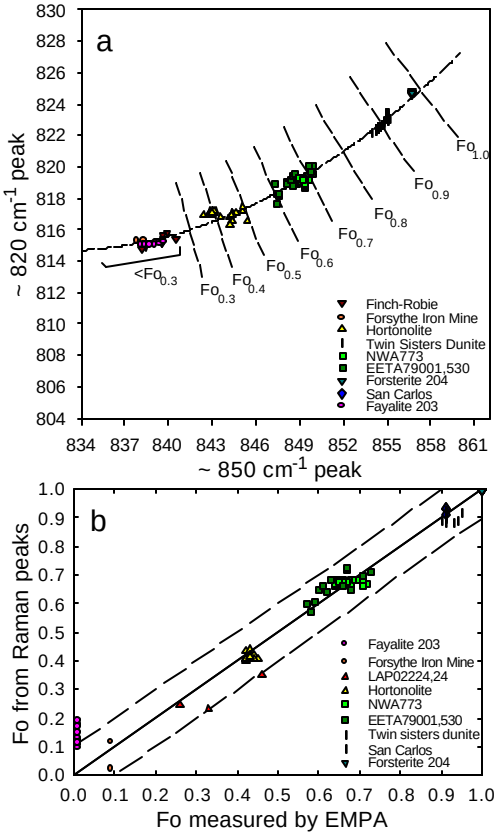

Fig. 2. a) 2-D plot for estimating olivine composition from peak positions. b) Comparison of Fo by EMPA to Fo estimated from Raman peak positions.

Discussion and conclusions. The sample data set (plus LAP) was used to test the calibration. We used the Raman peak positions with Eq. 1 to find the predicted Fo values and plotted them against the Fo values determined by EMPA. This comparison is presented in Figure 2b with the best-fit line that yields a 1:1 correlation (slope = 0.99). The greatest deviations occur at fayalitic compositions ($Fo_{<0.10}$) but most data are within ± 0.1 Fo units, illustrating that it is possible to use the positions of the olivine doublet to estimate most Fo-Fa olivine compositions with reasonable accuracy. The only data from intermediate compositions that stray from the best-fit line are 2 points from LAP. The discrepancy can be partly attributed to the different compositions "seen" by the two techniques in samples that are zoned on a fine scale because the techniques sample different volumes. However, zoning on a fine scale also produces broader and less well resolved peaks due to the overlapping of mode frequencies. EMPA indicates zoning from $Fo_{0.26}$ to $Fo_{0.46}$ in LAP within 75 μm. Nevertheless, Fo estimates from the Raman peak positions are within ± 0.15 of that determined by EMPA. Similarly, EETA79001,530 olivine peak positions scatter more than those of lunar sample NWA773. Both samples have cores of similar composition but the olivine doublets in EETA are broader and overlap more. We attribute the breadth of the peaks in the EETA xenocrysts to zoning at their rims due to reaction with the groundmass (ave. rim Fo= 0.61, ave. core= 0.73). This olivine calibration has improved our ability to extract compositional information more accurately from Raman spectra.

Table 1. Samples	type of sample	ave. Fo
Fayalite 203 [9]	synthetic, HUPS 401	0.01
Finch-Robie*	synthetic	no EMPA
Forsythe Iron Mine, Quebec, Canada* [19-21]	magnetite-bearing iron ore	0.09
LAP02224,24 [22-24]	lunar meteorite, basalt paired with LAP02205	0.26-0.46
Rustenberg, Transvaal, S. Africa*	Hortonolite	0.42
NWA 773 [25-26]	lunar meteorite, breccia w/ olivine gabbro clasts	0.67
EETA79001,530 [5, 27-29]	SNC meteorite, basaltic shergottite, xenocrysts	rims 0.61 core 0.73
San Carlos, Arizona, USA* [15, 30-33]	large polished forsterite grains	0.89
Twin Sisters Range, Washington, USA [34-35]	dunite	0.91
Forsterite 204 [8, 10, 15]	synthetic, HUPS 433	1.00

*samples from A. Hofmeister

Acknowledgements: Work supported by NASA grants NAG5-12114, NAG5-10703, & NAG5-12684. **References:** [1] Morris et al. (2004) *Science* **305**, 833-836. [2] McSween (2004) *Science* **305**, 842-845. [3] Christensen et al. (2004) *Science* **305**, 837-841. [4] Wang et al. (2001) *Am. Min.* **86**, 790-806. [5] Wang et al. (2004) *J.Raman Spec.* **35**, 504-514. [6] Kuebler et al. (2003) *LPSCXXXIV* 1953. [7] Kuebler et al. (2004) *LPSCXXXV* 1819. [8] Takei (1974) *J.Crystal Growth* **23**, 121-124. [9] Takei (1978) *J.Crystal Growth* **43**, 463-468. [10] Ishii (1978) *Am. Min.* **63**, 1198-1208. [11] Piriou & McMillan (1983) *Am. Min.* **68**, 426-443. [12] Chopelas (1991) *Am. Min.* **76**, 1101-1109. [13] Hofmeister (1987) *Phys. Chem. Min.* **14**, 499-513. [14] Paques-Ledent & Tarte (1973) *Spectrochim. Acta* **29A**, 1007-1016. [15] Guyot (1986) *Phys. Chem. Min.* **13**, 91-95. [16] Lam et al. (1990) *Am. Min.* **75**, 109-119. [17] Kuebler et al. (2001) *LPSCXXXII* 1697. [18] Sharma & Cooney (1990) *EOS* **71**, 525. [19] Jambor et al. (2002) *Environmental Geology* **43**, 1-17. [20] Machamer (1959) Master's thesis, McGill University. [21] Hogarth (1983) *CIM Bulletin* **76**, 75-84. [22] Jolliff et al. (2004) *LPSCXXXV* 1438. [23] Korotev (2004) *LPSCXXXV* 1416. [24] Satterwhite & Righter, eds. (2003) *Antarctic Meteorite News* **26**, no. 2. [25] Jolliff et al. (2003) *GCA* **67**, 4857-4879. [26] Fagan (2003) *MAPS* **38**, 529-554. [27] Steele & Smith (1982) *LPSCXIII* 764-765. [28] McSween & Jarosewich (1983) *GCA* **47**, 1501-1513. [29] Meyer (1996) *Mars Meteorite Compendium*, JSC Report 27672, Houston, TX. [30] Guyot (1996) *Physics of the Earth & Planetary Interiors* **98**, 17-29. [31] Awad et al. (2000) *GCA* **64**, 1765-1772. [32] Pokrovsky and Schott (2000) *GCA* **64**, 3313-3325. [33] Oelkers (2001) *Chemical Geology* **175**, 485-494. [34] Onyeagocha (1978) *GSA Bulletin* **89**, 1454-1474. [35] Ragan (1963) *Am. J. Science* **261**, 549-565.